Supplemental Material to the Manuscript "Radio frequency magnetometry using a single electron spin"

M. Loretz[1], T. Rosskopf[1], C. L. Degen[1]

[1]Department of Physics, ETH Zurich, Schafmattstrasse 16, 8093 Zurich, Switzerland.

1. Experimental setup

1.1. Optical and microwave components

Experiments were carried out at room temperature on a home-built confocal microscope. Single NV centers were excited by a $< 3\,\mathrm{mW}$, 532 nm laser pulse gated by an acousto-optic modulator in a double-pass arrangement. Luminescent photons were collected by an avalanche photo diode over an effective filter bandwidth of 630-800 nm, and counted using a standard PCI counter card (National Instruments, NI6602).

Microwave pulses were generated by an arbitrary waveform generator (Tektronix AWG5002C, 600 MS/s, 14 bits) at an IF of 100 MHz and upconverted to the desired $\sim 3.2\,\mathrm{GHz}$ using an I/Q mixer (Marki Microwaves, IQ-1545) and a low-phase-noise LO (Phasematrix, Quicksyn FSW-0020). The microwave power level was adjusted during numerical synthesis of the arbitrary waveform. The microwave signal was amplified by a linear power amplifier (Minicircuits ZHL-16W-43+) and the MHz rf probe field (HP 33120A) added using a bias-T (Customwave CMCH0674A). Microwaves were delivered by passing current through a lithographically patterned stripline in close proximity ($< 100\ \mu\mathrm{m}$) to the sample and terminated in a high-power $50\,\Omega$ terminator. From the narrow spectra observed (<10 kHz at 8 MHz Rabi frequency) we conclude that microwave power was stable to better than 0.5% over an entire experiment (∼hours). Rabi frequencies were independently calibrated using a series of Rabi nutations. The absolute calibration error was on the order of ±3%. For better absolute accuracy, an rf probe field of known frequency can be used as reference signal.

1.2. Pulse-timing diagram

Fig. A depicts the pulse-timing diagram used for spin lock experiments. At the start of each detection sequence, the spin is initialized into the $m_s = 0$ state using a 1 μs green laser pulse (not shown). A sequence of three linear frequency or amplitude sweeps of ~ 1 μs duration each is used to adiabatically transfer the spin into $|x+\rangle$ state. The reverse sequence is used to transfer $|x+\rangle$ ($|x-\rangle$) states back to $|0\rangle$ ($|1\rangle$) polarization. The polarization is detected using a second ~ 1 μs green laser pulse (not shown). Along with each signal, two reference signals were recorded to calibrate the luminescence of the $m_s = 0$ and $m_s = +1$ states. The overall efficiency of the adiabatic sweep sequence was $> 95\%$. The entire sequence was repeated millions of times until typically 10′000

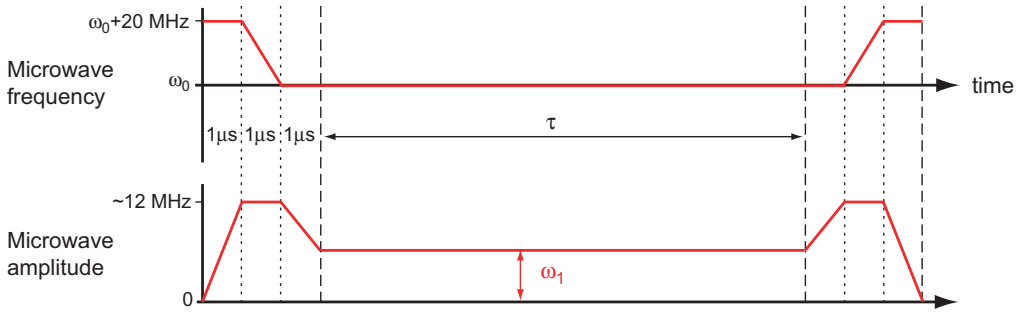

Figure A: Pulse-timing diagram for spin-lock experiments

photons were collected per point.

2. Transition probability

The transition probability may be analyzed for situtations where the excitation is coherent (infinite coherence time t_c), strongly correlated ($t_c \gg \tau$), or uncorrelated ($t_c \ll \tau$), where τ is the evolution time (spin lock duration).

2.1. Coherent excitation ($t_c = \infty$)

The transition probability of a two-level system with energy spacing ω_1 subject to a coherent, harmonic driving field of frequency Ω and amplitude Ω_1 is given by [S1]

$$p = p_0 \frac{\Omega_1^2}{\Omega_{\text{eff}}^2} \sin^2(\Omega_{\text{eff}}\tau/2) \tag{1}$$

$$\approx \frac{p_0}{4}\Omega_1^2\tau^2 \qquad \text{(for weak fields, } \Omega_1\tau \ll \pi/2) \tag{2}$$

where $p_0 \leq 1$ is the maximum possible transition probability and $\Omega_{\text{eff}} = \sqrt{\Omega_1^2 + (\Omega - \omega_{\text{eff}})^2}$. This is Eq. (1) in the main manuscript.

2.2. Stochastic excitation, correlated ($t_c \gg \tau$)

This is the situation of a driving field with a slowly varying amplitude. Since $t_c \gg \tau$, we can assume that the amplitude Ω_1 is constant during interrogation time τ but varies between interrogation periods. If we assume that Ω_1 has a normal distribution (for example, it is generated by a large number of independent fluctuators, such as precessing nuclear spins), and neglecting detuning ($\Omega_{\text{eff}} = \Omega_1$), the transition probability is

$$p = \int_{-\infty}^{\infty} d\Omega_1 p(\Omega_1) \frac{1}{\sqrt{2\pi}\Omega_{\text{rms}}} e^{-\frac{\Omega_1^2}{2\Omega_{\text{rms}}^2}} \tag{3}$$

$$= \int_{-\infty}^{\infty} d\Omega_1 p_0 \sin(\Omega_1\tau/2)^2 \frac{1}{\sqrt{2\pi}\Omega_{\text{rms}}} e^{-\frac{\Omega_1^2}{2\Omega_{\text{rms}}^2}} \tag{4}$$

$$= \frac{p_0}{2}\left(1 - e^{-\frac{1}{2}\Omega_{\text{rms}}^2\tau^2}\right) \tag{5}$$

$$\approx \frac{p_0}{4}\Omega_{\text{rms}}^2\tau^2 \qquad \text{(for weak fields, } \Omega_{\text{rms}}\tau \ll \pi/2) \tag{6}$$

Ω_{rms} is the rms amplitude of the fluctuating magnetic field. A nominal rotating-frame relaxation time $T_{1\rho}$ is found by setting $e^{-\frac{1}{2}\Omega_{\text{rms}}^2 T_{1\rho}^2} = 1/e$, thus $\frac{1}{2}\Omega_{\text{rms}}^2 T_{1\rho}^2 = 1$ and $T_{1\rho} = \sqrt{2}/\Omega_{\text{rms}}$.

2.3. Stochastic excitation, uncorrelated ($t_c \ll \tau$)

This is the situation derived in classical magnetic resonance textbooks [S2]. The transition probability is given by

$$p = \frac{p_0}{2}\left(1 - e^{-\tau/T_{1\rho}}\right), \text{ where } T_{1\rho}^{-1} = \frac{1}{4}\gamma^2 S_B(\omega). \tag{7}$$

γ is the electronic gyromagnetic ratio. If the noise is centered around zero frequency and $\omega < t_c^{-1}$, as for many lifetime-limited processes, the spectral density is frequency independent, $S = 2\Omega_{\text{rms}}^2 t_c$, and the transition probability is given by

$$p = \frac{p_0}{2}\left(1 - e^{-\frac{1}{2}\Omega_{\text{rms}}^2 t_c\tau}\right) \tag{8}$$

$$\approx \frac{p_0}{4}\Omega_{\text{rms}}^2 t_c\tau \qquad \text{(for weak fields, } \Omega_{\text{rms}}\tau \ll \pi/2) \tag{9}$$

3. Linewidth

Linewidth in rotating-frame magnetometry is determined by three parameters: Spin lock duration τ, magnetic field power in the vicinity of the detection frequency, and inhomogeneous broadening of the electron spin resonance transition. Each parameter imposes a limit on the linewidth, and the largest of the three contributions will set the experimentally observed linewidth.

3.1. Time-limited linewidth

Short τ lead to a wider detection bandwidth (in analogy to lifetime-limited processes). If we denote detector bandwidth by b, and define it as twice the frequency offset $\Omega - \omega_1$ for which the probability function p [Eq. (2)] is reduced to 50% of the maximum value,

$$\frac{p(\Omega - \omega_1 = b/2)}{p(\Omega - \omega_1 = 0)} = 0.5 \tag{10}$$

we can numerically solve for b to find:

$$b = 5.5680\,\tau^{-1} \tag{11}$$

This relation applies for weak magnetic fields ($\Omega_1 < \tau^{-1}$) where power broadening is small. An example for an evolution-time-limited linewidth is shown by the blue curve in Fig. B, where $\Omega_1 = \frac{\pi}{4}\tau^{-1}$.

3.2. Power-limited linewidth

Large magnetic probe fields will saturate the detector and lead to power broadening. The condition for power broadening is $\Omega_1 > \tau^{-1}$, and in this case, the detection bandwidth is dominated by the Lorenzian factor in p [Eq. (2)]. The power-broadened detector bandwidth is:

$$b = 2\Omega_1 \tag{12}$$

An example for a power-broadened linewidth is shown by the red curve in Fig. B, where $\Omega_1 = (5\pi)\tau^{-1}$. The detector bandwidth is given by the full-width-at-half-maximum of the envelope (dashed curve).

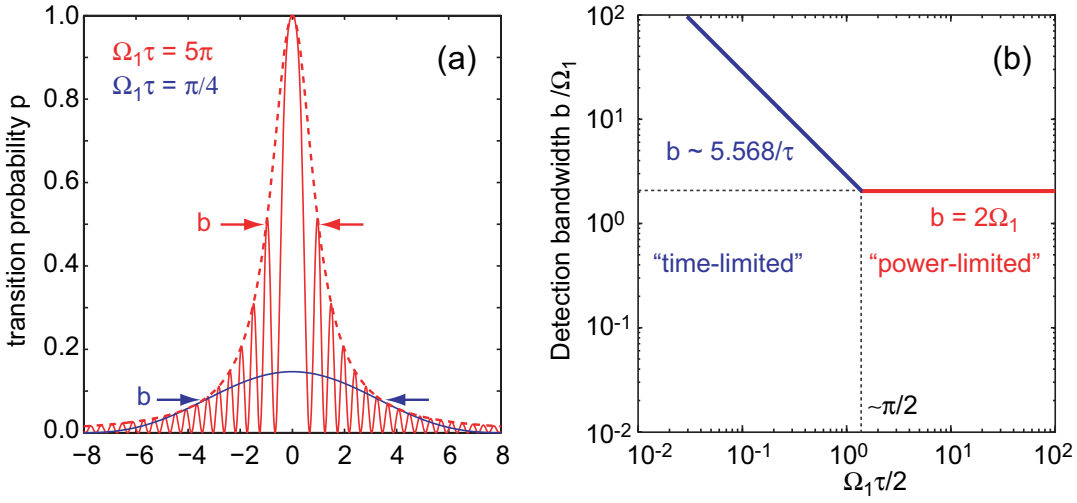

Figure B: (a) Eq. (2) plotted as a function of detuning $\Omega - \omega_{\text{eff}}$ for an evolution-time-limited situation (blue, $\Omega_1\tau = \pi/4$) and a power-broadened situation (red, $\Omega_1\tau = 5\pi$). Dashed red line is the envelope. (b) Detection bandwidth b plotted as a function of $\Omega_1\tau$, indicating the two linewidth regimes.

3.3. Inhomogeneously broadened linewidth

A third line broadening mechanism is through fluctuations in the effective Rabi frequency $\omega_{\text{eff}} = \sqrt{\omega_1^2 + (\omega - \omega_0)^2}$, which may be caused by fluctuations in microwave power, microwave frequency, or the Larmor frequency of the electron spin.

3.3.1. Fluctuations in microwave power

Fluctuations in microwave power P lead to fluctuations in the microwave amplitude $\omega_1 \propto \sqrt{P}$. Specifically, a variation of δP in microwave power P will lead to variation of $\delta\omega_1 \approx \omega_1(\delta P/2P)$ in detector frequency. Since power fluctuations can occur with microwave generation, they are a potential concern. We have not calibrated power stability for our microwave generation, but from the fact that narrow spectra ($< 10\,\text{kHz}$) were observed at a detector frequency of 7.5 MHz we can deduce that power stability was better than $\delta P/P \lesssim 2 \cdot (10\text{kHz}/7.5\text{MHz}) \approx 0.3\%$ for these experiments.

3.3.2. Jitter in microwave frequency

Jitter in microwave frequency is negligible.

3.3.3. Inhomogeneous broadening of ESR linewidth

Fluctuations in the electron spin Larmor frequency ω_0, due to inhomogeneous broadening of the ESR linewidth, lead to an associated line broadening in the rotating-frame spectrum. Typically, as is shown in the following, the rotating-frame line broadening is reduced by $\propto \frac{\sigma_{\omega_0}}{\omega_1}$ compared to the original ESR linewidth, where σ_{ω_0} is the ESR linewidth and ω_1 the Rabi frequency.

We show this for the specific situation where the EPR spectrum $q(\omega_0)$ is described by a Gaussian:

$$q(\omega_0) = \frac{1}{\sigma_{\omega_0}\sqrt{2\pi}} \exp\left[-\frac{(\omega - \omega_0 - \Delta\omega_0)^2}{2\sigma_{\omega_0}^2}\right]. \tag{13}$$

Here, $\Delta\omega_0$ is the mean detuning and σ_{ω_0} the sigma of the resonance. (For the ^{14}NV center, three Gaussians were added to reproduce the three hyperfine resonances). Since $q(\omega_0)$ is a Gaussian, the modified transition probability $\tilde{p}$ is also approximately a Gaussian, with a peak shift $\Delta\omega_1$ given by

$$\Delta\omega_1 = \omega_1 - \omega_{\text{eff}} \approx \omega_1 - \omega_1\left(1 + \frac{\Delta\omega_0^2}{2\omega_1^2}\right) \approx -\frac{\Delta\omega_0^2}{2\omega_1}, \tag{14}$$

where $\omega_{\text{eff}} = \sqrt{\omega_1^2 + (\omega - \omega_0)^2}$, and a sigma σ_{ω_1} given by

$$\sigma_{\omega_1}^2 = \left(\frac{\partial\Delta\omega_1}{\partial\Delta\omega_0}\right)^2 \sigma_{\omega_0}^2 + \left(\frac{\sigma_{\omega_0}^2}{2\omega_1}\right)^2 \tag{15}$$

$$= \left[\frac{\Delta\omega_0^2}{\omega_1^2} + \frac{\sigma_{\omega_0}^2}{4\omega_1^2}\right]\sigma_{\omega_0}^2. \tag{16}$$

The above equations assume that $\Delta\omega_0, \sigma_{\omega_0} \ll \omega_1$ (which applies to the experiments presented here). The according inhomogeneous linewidth b_{inh} is

$$b_{\text{inh}} = \sqrt{8\ln(2)}\sigma_{\omega_1} \approx 2.35\sigma_{\omega_1} \tag{17}$$

For example, for an ESR linewidth with $\sigma_{\omega_0}/(2\pi) \approx 350\,\text{kHz}$ and zero detuning ($\Delta\omega_0 = 0$), as well as a Rabi frequency of $\omega_1/(2\pi) = 7.5\,\text{MHz}$, the associated linewidth of the rotating frame has a sigma of approximately $\sigma_{\omega_1}/(2\pi) = 7.7\,\text{kHz}$ (see Table 2). The corresponding full-width-at-half-maximum value is $b_{\text{inh}} \approx 2.35 \cdot 7.7\,\text{kHz} \approx 18\,\text{kHz}$. Since we were able to observe linewidths $< 10\,\text{kHz}$, the original EPR linewidth is probably overestimated.

4. Sensitivity

Sensitivity of rotating-frame magnetometry is influenced by several parameters: Spin lock duration τ, magnetic background noise (described by a finite relaxation time $T_{1\rho}$), efficiency of the optical read-out (including shot noise and optical contrast), and inhomogeneous broadening of the ESR transition.

4.1. Interrogation time

Spin-lock duration directly determines the transition probability between the two quantum states (see Section 2.). For weak fields, the transition probability is approximately [see Eq. (2)]:

$$p = \frac{1}{4} p_0 \Omega_1^2 \tau^2 \tag{18}$$

where p_0 is peak contrast, Ω_1 the amplitude of the magnetic field to detect, and τ spin lock duration.

4.2. Magnetic background noise

Magnetic noise at the detector is typically dominated by the fluctuating bath of spins surrounding the electronic spin sensor. For NV centers in diamond these spins may be ^{13}C lattice nuclei, N donors, or surface impurities. Magnetic noise at the detector is the most fundamental noise source and sets a lower limit to the minimum detectable field.

In the experiment, magnetic background noise is observed as rotating-frame relaxation, reducing p_0 for evolution times τ approaching $T_{1\rho}$ (according to Eq. 7). If rotating-frame relaxation needs to be taken into account, p_0 must hence be substituted by $p_0 \to p_0 e^{-\frac{\tau}{T_{1\rho}}}$.

4.3. Optical read-out efficiency

The dominant measurement noise in our measurement comes from shot noise in the optical read-out of the spin state, due to the finite number of photons collected per point. For a total number of photons collected C, the shot noise is $\sigma_C = \sqrt{C}$. The total number of photons detected C is

$$C = Nr = (T/t_{\text{meas}})r \tag{19}$$

where N is the number of measurements, r is the number of photons collected per measurement (collection efficiency), T is the total measurement time, and t_{meas} is the duration of one measurement ($t_{\text{meas}} \gtrsim \tau$).

The shot-noise limited signal-to-noise ratio is given by

$$\text{SNR} = \frac{\Delta C}{\sqrt{C}} = p\epsilon\sqrt{C} \approx p\epsilon\sqrt{\frac{Tr}{\tau}} \tag{20}$$

where C is the number of photons detected, $\Delta C = p\epsilon C$ is the change in photon counts due to the magnetic probe field ($\Delta C \ll C$), and ϵ the optical contrast between $|0\rangle$ and $|1\rangle$ spin states.

4.4. Inhomogeneous line broadening

Inhomogeneous broadening of the rotating-frame linewidth (see Section 3.3.3.) reduces the peak transition probability p if it is the largest contribution to the rotating-frame linewidth. Specifically, if the sensor has a detector bandwidth of b (either time- or power-limited) an inhomogeneously broadened linewidth $b_{\text{inh}} > b$, then peak probability is reduced by a factor $x = b/b_{\text{inh}}$. (This can be understood as a convolution between the two spectral functions with fixed areas under each curve.)

4.5. Overall Sensitivity

Collecting equations from Sections 4.1-4.4 and using $\Omega_1 = \gamma B_1^{\mathrm{rf}}$, where γ is the electron gyromagnetic ratio, the overall SNR for magnetic field sensing becomes:

$$\mathrm{SNR} = \frac{1}{4} x p_0 e^{-\frac{\tau}{T_{1\rho}}} \epsilon (\gamma B_1^{\mathrm{rf}})^2 \tau^{1.5} (Tr)^{0.5}. \tag{21}$$

The corresponding minimum detectable field (for unit SNR) is:

$$B_{\min} = \left[\frac{1}{4} x p_0 e^{-\frac{\tau}{T_{1\rho}}} \epsilon \gamma^2 \tau^{1.5} (Tr)^{0.5} \right]^{-0.5}. \tag{22}$$

Alternatively, one can experimentally infer the minimum detectable field from the standard deviation σ_p of the baseline noise of the transition probability.

$$\sigma_p = \frac{p_0}{4} \gamma^2 B_{\min}^2 \tau^2. \tag{23}$$

Solving for $B_{\min}$,

$$B_{\min} = \frac{2}{\gamma \tau} \sqrt{\frac{\sigma_p}{p_0}} \tag{24}$$

For the last two equations, as well as sensitivity values reported in Table 1, it was assumed that $x = 1$ and $\tau \ll T_{1\rho}$.

5. Calculations and fits to experimental data

5.1. Coherent oscillations between $|x+\rangle$ and $|x-\rangle$ (Figure 2)

The oscillation in Fig. 2 was fit to

$$p = \frac{p_0}{2} \left(1 - e^{-t^2/(2T)} \cos(\Omega_1 t) \right). \tag{25}$$

(This equation is equivalent to Eq. (1) in the main manuscript, except for that a Gaussian decay was added). Here, p_0 is contrast, Ω_1 is the oscillation frequency, and T a Gaussian decay constant. The fit yielded $p_0 = 0.56$, $\Omega_1/(2\pi) = 46.1\,\mathrm{kHz}$, and $T = 28\ \mu\mathrm{s}$.

The decaying sinusoid can also be directly calculated from Eqs. (1), (4) and (5) in the main manuscript for an inhomogeneously broadened ESR transition. Specifically, we can calculate $p(\tau, \Omega)$ as a function of evolution time τ and RF frequency offset $\Omega - \omega_1$, and then integrate over Ω assuming a Gaussian distribution of offsets $\Omega - \omega_1$:

$$\tilde{p}(\tau) = \int_{-\infty}^{\infty} d\Omega \left(\frac{1}{\sigma_{\omega_1} \sqrt{2\pi}} \exp\left[-\frac{(\Omega - \omega_1 - \Delta\Omega_0)^2}{\sigma_{\omega_1}^2} \right] \right) p(\tau, \Omega). \tag{26}$$

Here, σ_{ω_1} is the inhomogeneous broadening (sigma) of the rotating-frame spectrum and $\Delta\Omega_0$ is the mismatch between Ω and ω_1. We have calculated $\tilde{p}(\tau)$ for the dataset shown in Fig. 2 in the main manuscript and find that $\sigma_{\omega_1}/(2\pi) \approx 15\,\mathrm{kHz}$ and $\Delta\Omega_0 \approx 30\,\mathrm{kHz}$ in this measurement.

5.2. Sensitivity (Figure 3)

The sensitivity was calculated in two ways. First, shot-noise limited sensitivity was calculated from experimental parameters. Second, the sensitivity was directly inferred from the standard deviation of the baseline in the transition rate spectra shown in Fig. 2(b,c). Parameters are collected in Table 1 and refer to Sections 4.2 and 4.3. All numbers are per point.

Quantity	Main spectrum in Fig. 2(b)	41-nT-spectrum in Fig. 2(c)
Evolution time τ	15 μs	300 μs
Single measurement duration t_{meas}	31.4 μs	316.4 μs
Total time T	145 s	840 s
Total counts C	9'700	10'200
Number of measurements N	$4.6 \cdot 10^6$	$2.7 \cdot 10^6$
Photons per measurement r	0.0021	0.0039
Contrast ϵ	0.31	0.31
Probability p_0	0.45	0.45
Baseline noise σ_p	0.029	0.020
B_{min} from shot noise [Eq. (22)]	170 nT	10 nT
B_{min} from baseline noise [Eq. (24)]	200 nT	8 nT

Table 1: Experimental parameters and magnetic field sensitivity B_{min} for spectra in Fig. 3(b,c).

5.3. Linewidth (Figure 3)

Experimental linewidths indicated for the 41-nT and 82-nT spectra in Fig. 3(c) are determined using a Gaussian fit and are reported as full width at half height (FWHH = 2.3548σ). Corresponding calculated linewidths reported in the text are determined by numerically finding the FWHH as explained in Section 3.1. The EPR-linewidth induced line broadening (Section 3.2.2) for these spectra is on the order of 8 kHz, see Table 2.

5.4. Spin-state-selection spectra (Figure 4)

The transition probability shown in Figures 4(a,c) was calculated as function of ω_1 for each hyperfine line separately, and the three probabilities then added (this is valid as long as there is no strong overlap between features).

The transition probability associated with a single hyperfine line was calculated according to Section 3.2.2. The mean detuning $\Delta\omega_0$ and linewidth σ_{ω_0} were obtained from Gaussian fits to the ODMR spectrum shown in Fig. 3(a). These values along with detuning $\Delta\omega_1$ and linewidth σ_{ω_1} of the rotating-frame spectrum are collected in Table 2.

^{14}N sublevel	ω_1	$\Delta\omega_0$	σ_{ω_0}	$\Delta\omega_1$	σ_{ω_1}
$m_I = -1$	8 MHz	-0.5 MHz	350 kHz	-16 kHz	22 kHz
$m_I = 0$	8 MHz	1.7 MHz	350 kHz	-180 kHz	74 kHz
$m_I = +1$	8 MHz	3.9 MHz	350 kHz	-950 kHz	170 kHz
—	8 MHz	0 MHz	350 kHz	0 kHz	7.7 kHz

Table 2: Line shift $\Delta\omega_1$ and linewidth σ_{ω_1} for experiments shown in Fig. 2(a) and Fig. 4(c) in the main manuscript. Lowest row is for an ideal situation of zero detuning.

5.5. T_1 and $T_{1\rho}$ relaxation times (Figure 5)

$T_{1\rho}$ relaxation time measurements used the pulse-timing diagram as shown in Figure A with a variable spin lock duration τ. T_1 relaxation time measurements used no microwaves at all and simply consisted on an initialization of the spin by a first green laser pulse, and readout of the spin state by a second green laser point after time τ. Relaxation time measurements were fitted to

$$p = p_0 \left(1 - e^{-t/T}\right), \tag{27}$$

where $p_0 = 1/3$ is contrast and T is the respective relaxation time (T_1 or $T_{1\rho}$).

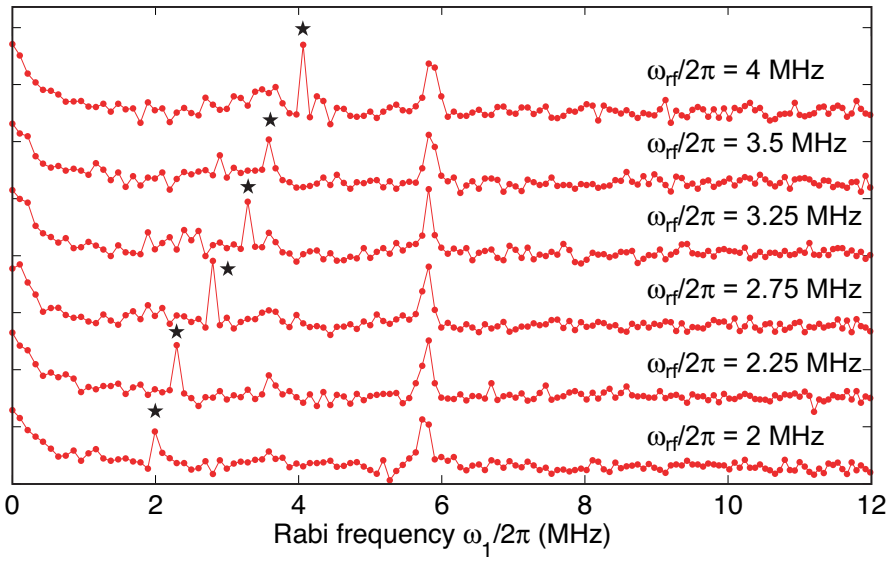

Figure C: Series of rotating-frame spectra for rf probe field frequencies $\Omega_1/2\pi$ between 2 and 4 MHz. Signal peaks are marked by $\star$.

6. Origin of the 6-MHz feature

This section collects experimental data on the peak that appeared between 5.5 and 6.2 MHz in Figs. 3 and 4. While we do not know the exact cause and mechanism resulting in this feature.

Experimental observations:

- The feature appeared at frequencies between approximately 5.2 MHz and 6.3 MHz, depending on the measurement.
- The feature was observed on three independent ^{14}NV centers. It was not observed on any ^{15}NV center.
- The feature is due to a coherent source, evidenced by oscillation similar to Fig. 2. Two measured oscillation frequencies were about 34 kHz and 17 kHz, respectively.
- The feature is present regardless whether the auxiliary RF signal line was connected or disconnected.
- The feature is related to the $m_I = -1$ nuclear spin state (as evident from Fig. 4). We have not observed any peaks related to $m_I = 0, +1$, but cannot exclude them with the given SNR.

Based on these observations we suspect that the feature is related to the ^{14}N nuclear spin of the NV center. One possible mechanism is through cross-terms in the Hamiltonian that result from a slight vector misalignment of the $10 - 20\,\mathrm{mT}$ bias field. Another mechanism is through the small perpendicular component of the dipolar hyperfine interaction [S3].

7. Additional measurements

Fig. C shows a series of spectra for rf probe field frequencies $\Omega_1/2\pi$ between 2 and 4 MHz, complementing the spectra shown in the main manuscript that were obtained at higher $\Omega_1/2\pi$. Magnitude of rf field was between 1 and 2 μT.

References

[S1] F. W. Cummings, Am. J. Phys. 30, 898 (1962).
[S2] C. P. Slichter, *Principles of Magnetic Resonance*, (Springer, Heidelberg, 1996).
[S3] S. Felton *et al.* Phys. Rev. B 79, 075203 (2009).